Silica-embedded silicon photonic crystal waveguides

T. P. White[1,*], L. O'Faolain[1], Juntao Li[1,2], L. C. Andreani[3], and T. F. Krauss[1]

[1.] *School of Physics and Astronomy, University of St Andrews, St Andrews, Fife, KY169SS, UK*
[2]. *State Key Laboratory of Optoelectronic Materials and Technologies, Sun Yat-sen University, Guangzhou 510275, China*
[3]. *Dipartimento di Fisica "A. Volta", Università di Pavia, Via Bassi 6, I-27100 Pavia, Italy*

** Corresponding author: tom.white@st-andrews.ac.uk*

Abstract: We report on the fabrication and characterization of silicon photonic crystal waveguides completely embedded in silica. These waveguides offer a robust alternative to air-membranes and are fully compatible with monolithic integration. Despite the reduced refractive index contrast compared to the air-membranes, these waveguides offer a considerable operating range of ≈10 nm in the 1550 nm window. While the reduced index contrast weakens the perturbations due to surface roughness, we measure losses of 35 ± 3dB/cm compared to 12 ± 3 dB/cm for nominally identical air-membranes. Numerical analysis reveals that the difference in loss results from the different mode distribution and group index of the respective waveguide modes. Radius disorder is used as a fitting parameter in the numerical simulations with the best fits found for disorder levels of 1.4 – 1.7 nm RMS, which attest to the high quality of our structures.

OCIS codes:: (130.5296) Photonic crystal waveguides. (230.3120) Integrated optics devices

References and Links

1. E. Kuramochi, M. Notomi, S. Hughes, A. Shinya, T. Watanabe, and L. Ramunno, "Disorder-induced scattering loss of line-defect waveguides in photonic crystal slabs," Phys. Rev. B. **72**, 161318 (2005).
2. L. O'Faolain, X. Yuan, D. McIntyre, S. Thoms, H. Chong, R. M. De la Rue, and T. F. Krauss, "Low-loss propagation in photonic crystal waveguides," Electron. Lett. **42,** 1454-1455 (2006).
3. M. Notomi, T. Tanabe, A. Shinya, E. Kuramochi, H. Taniyama, S. Mitsugi, and M. Morita, "Nonlinear and adiabatic control of high-*Q* photonic-crystal nanocavities," Opt. Express **15**, 17458-17481 (2008).
4. M. Settle, M. Salib, A. Michaeli, and T. F. Krauss, "Low loss silicon on insulator photonic crystal waveguides made by 193nm optical lithography," Opt. Express **14**, 2440-2445 (2006).
5. Y. Tanaka, T. Asano, R. Hatsuta, and S. Noda, "Analysis of a line-defect waveguide on a silicon-on-insulator two-dimensional photonic-crystal slab," J. Lightwave. Technol. **22**, 2787-2792 (2004).
6. M. Notomi, A. Shinya, S. Mitsugi, E. Kuramochi, and H. Ryu, "Waveguides, resonators and their coupled elements in photonic crystal slabs," Opt. Express **12**, 1551-1561 (2004).
7. D. Gerace and L. C. Andreani, "Low-loss guided modes in photonic crystal waveguides," Opt. Express **13**, 4939-4951 (2005).
8. See http://www.nanophotonics.eu.
9. C-C. Yang and W-C Chen, "The structures and properties of hydrogen silsesquioxane (HSQ) films produced by thermal curing," J. Mater. Chem. **12**, 1138–1141 (2002).
10. Y. A. Vlasov and S. J. McNab, "Losses in single-mode silicon-on-insulator strip waveguides and bends," Opt. Express **12**, 1622-1631 (2004).
11. L. C. Andreani and D. Gerace, "Light-matter interaction in photonic crystal slabs," Phys. Status. Solidi B **244**, 3528-3539 (2007).
12. L. O'Faolain, T. P. White, D. O'Brien, X. Yuan, M. D. Settle, and T. F. Krauss, "Dependence of extrinsic loss on group velocity in photonic crystal waveguides," Opt. Express **15**, 13129-13138 (2007).
13. D. Gerace and L. C. Andreani, "Disorder-induced losses in photonic crystal waveguides with line defects," Opt. Lett. **29**, 1897-1899 (2004).
14. M. Notomi, A. Shinya, K. Yamada, J. Takahashi, C. Takahashi, and I. Yokahama, "Structural tuning of guiding modes of line-defect waveguides of silicon-on-insulator photonic crystal slabs," IEEE J. Quantum Electron. **38**, 736-742 (2000).

#101180 - $15.00 USD Received 5 Sep 2008; revised 8 Oct 2008; accepted 8 Oct 2008; published 10 Oct 2008

1. Introduction

Planar photonic crystal devices based on waveguides, cavities and other basic components have been proposed for various applications including switches, modulators, delay lines and on-chip interconnects. For many of these, silicon is the preferred material due to its optical properties and the potential for integration with electronics. To date, most experimental studies of Si PhC waveguides have focused on membrane or asymmetric silica-clad structures. Membrane PhCs consist of a thin (typically 200-240 nm) layer of silicon with air above and below. This geometry provides two important features; a high index contrast for strong out-of-plane confinement, and a symmetric cladding that ensures orthogonality of the TE-like and TM-like slab modes. The lowest PhC waveguide losses have been achieved for membrane structures, with several groups reporting values below 5 dB/cm [1-3]. Membranes, however, are easily damaged and susceptible to contamination from the environment. They are also difficult to integrate with other components such as heaters or electronic control circuitry.

A more robust alternative is to retain the silica substrate beneath the silicon, creating an asymmetric structure with air above. In addition to the improved mechanical stability, this silicon-on-insulator (SOI) geometry can be fabricated entirely using CMOS fabrication methods [4], and is thus more suited to monolithic integration with electronics than membrane structures. From an optical perspective, however, such asymmetric SOI PhCs have several disadvantages. First, the silica light line is lower than that of air so the operating bandwidth is reduced. Second, the silica cladding breaks the vertical symmetry of the structure, allowing coupling between the TE-like and TM-like modes of the silicon slab, thus increasing propagation loss and further reducing the useful transmission bandwidth [5]. Propagation losses below 15 dB/cm have been reported for asymmetric-clad SOI PhC waveguides, with bandwidths of less than 10 nm [4, 6].

Here we introduce a third, oxide-clad, geometry, in which the silicon guide layer is fully embedded in silica. Numerical results suggest that this geometry can support low loss PhC waveguides with bandwidths exceeding 20 nm [7], but no experimental loss measurements have yet been published to our knowledge.

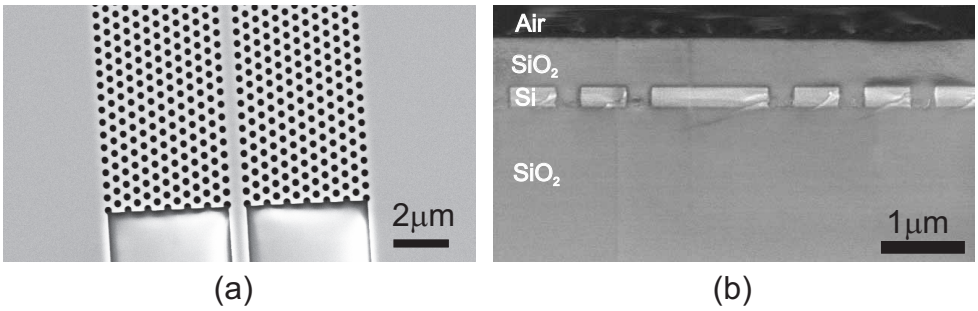

Fig. 1.(a) Scanning electron micrograph (SEM) of a W1 waveguide (without the oxide cladding) and the tapered access waveguide. (b) SEM showing a cross-section of an oxide-clad PhC. The flowable oxide (FOx) layer is clearly visible in the holes and above the Si layer.

2. Fabrication

Two sets of W1 waveguides were processed simultaneously to ensure that there was no systematic variation in disorder between samples, enabling a direct comparison of the propagation losses in membrane and oxide-clad structures. Each set consisted of PhC waveguides with lengths ranging from 100 μm to 1900 μm, coupled to 3 μm wide ridge access waveguides via a tapered waveguide section. The devices were fabricated on a SOITEC SOI wafer comprising a nominally 220 nm thick Silicon layer on 2 um of silica. The sample was spun with ZEP520A electron beam resist and the pattern exposed using a hybrid

#101180 - $15.00 USD Received 5 Sep 2008; revised 8 Oct 2008; accepted 8 Oct 2008; published 10 Oct 2008

ZEISS GEMINI 1530/RAITH ELPHY electron beam writer at an acceleration voltage of 30 KeV. The resist was developed using xylene with ultrasonic agitation and the pattern was transferred to the Silicon layer via Reactive Ion Etching with CHF3 and SF6 gases, using a carefully optimized etching regime. The fabrication process is very similar to that of [2] and was carried out in the framework of the ePIXnet Nanostructuring Platform for Photonic Integration [8].

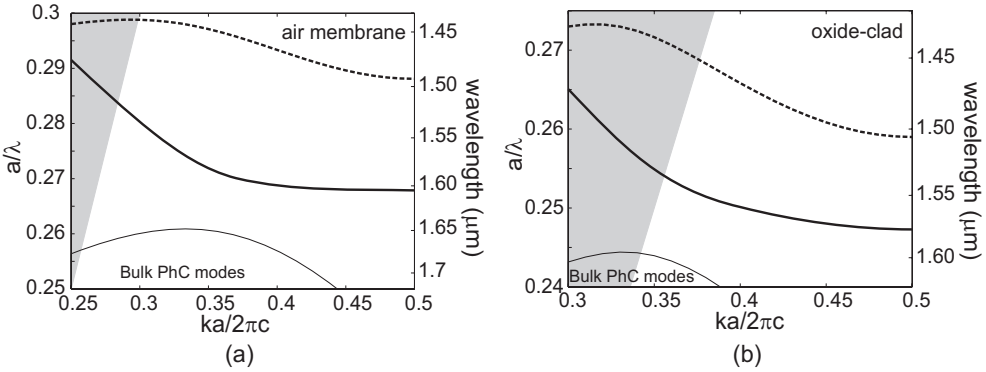

Fig. 2. Dispersion curves of the W1 PhC waveguides calculated using the GME method with the parameters given in the text. (a) Air membrane. (b) Oxide-clad. Solid (dashed) lines refer to the even (odd) defect mode, respectively. The shading indicates the region above the lightline for (a) air and (b) silica cladding.

Following lithography and etching, the membrane PhC waveguides were created by selectively etching the oxide cladding from beneath the PhC with dilute HF acid solution. The oxide-clad PhC waveguides were not membraned, but instead, a flowable oxide (FOx) containing hydrogen silsesquioxane (commercially available FOX-14 from Dow Corning) was spun onto the structures after reactive ion etching and resist removal. The sample was initially baked at 100°C to drive off the solvent and then hard baked at 400°C for 4 hours. The resulting oxide cladding has a thickness of approximately 500nm as shown in the cross-section scanning electron micrograph image in Fig. 1(b). Many of the relevant properties of HSQ have been studied in [9] and references therein. While the SEM inspection shows good penetration of the FOx into the holes, it is difficult to determine the quality of the in-filling due to damage when cleaving through the PhC structure. However the good agreement of the measured and calculated loss spectra shown in Fig. 3 is strong evidence that the holes are back-filled with oxide. Furthermore, irregular filling would increase the disorder of the structure, and hence we would expect significantly higher losses.

Due to the different index profiles of the two geometries, slightly different lattice parameters were used to achieve operation in the 1550 nm window. The membrane PhC waveguides had a lattice period of a = 430 nm and a hole radius of r = 127 nm, corresponding to r/a = 0.295, while the oxide-clad PhC waveguides had a = 390 nm and r = 98 nm (r/a = 0.250). Figure 2 shows the corresponding bandstructures for these parameters, calculated using a guided-mode expansion (GME) method [7] with refractive indices of n_{Si}=3.48 and n_{silica}=1.4. Note that the portion of the fundamental (or even) defect mode lying below the light line is truly single-mode in both structures, as the odd defect mode lies at higher frequencies.

3. Cut-back loss measurements

To measure the propagation loss, the TE-polarization transmission spectrum of each waveguide was first measured using a broadband LED light source and an optical spectrum analyzer. Light was coupled into the access waveguides using a free-space characterization setup consisting of a polarizing beam splitter and two microscope objectives to focus the light onto the input facet and collect it at the output facet. The propagation loss of the PhC

#101180 - $15.00 USD Received 5 Sep 2008; revised 8 Oct 2008; accepted 8 Oct 2008; published 10 Oct 2008

waveguides was then determined via the cut-back method, taking into account the losses in the ridge access waveguides, which were measured separately as 4 ± 2dB/cm with the oxide cladding, and 5 ± 2dB/cm without the cladding.

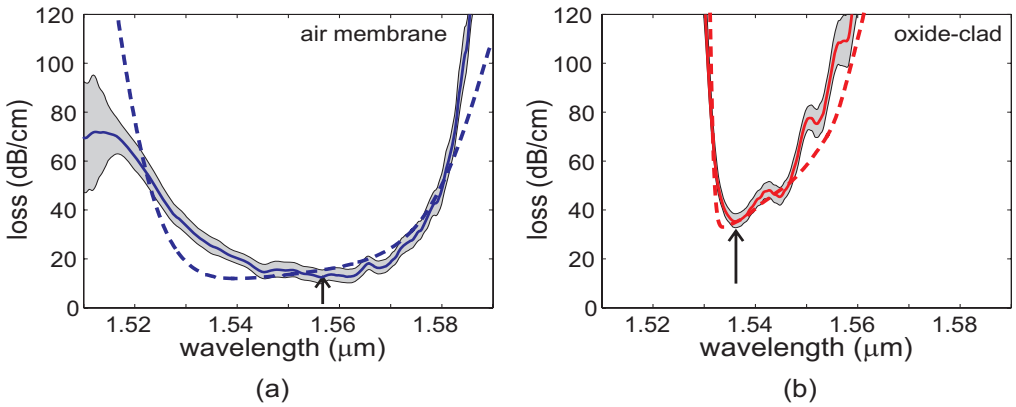

Fig. 3. Propagation loss spectra for (a) air membrane PhC waveguides and (b) oxide-clad PhC waveguides. Solid curve and shaded region: measured loss and experimental uncertainty respectively. The arrows indicate the minimum loss wavelengths. Dashed curves: loss spectra calculated using the GME method for a radius disorder of Δr = 1.7 nm in (a) and 1.4 nm in (b).

Figure 3 shows the measured loss as a function of wavelength for the two geometries, where the shaded grey region is given by the combined uncertainties of the ridge waveguide loss and the linear regression analysis of the cutback data. The dashed curves show the calculated loss spectrum as described in Section 4. We measure minimum losses of 12 ± 3 dB/cm at λ = 1557 nm and 35 ± 3 dB/cm at λ = 1536nm respectively for the air membrane and oxide-clad PhCs, indicated by arrows in Fig. 3. Figure 4 shows the corresponding cut-back data at these two points for waveguides up to 1.9 mm in length. The transmission axis shows the fiber-fiber transmission, and thus includes the free-space coupling losses of the measurement setup.

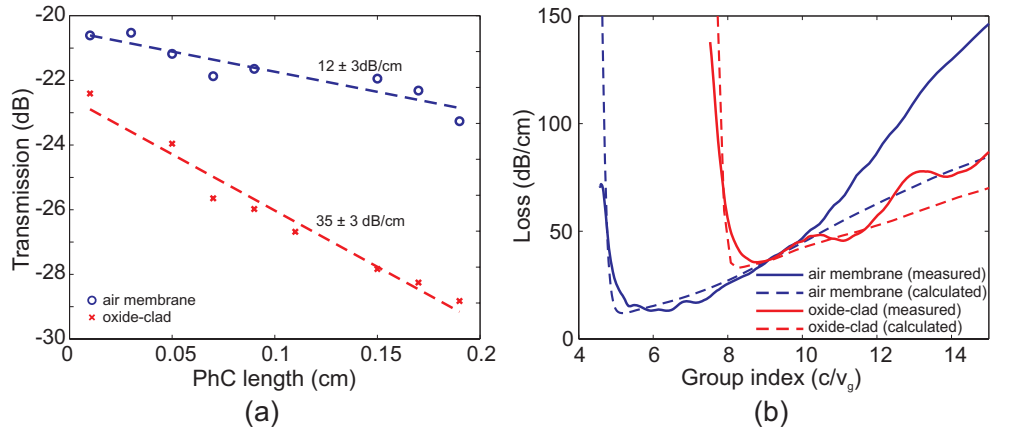

Fig. 4. (a) Cutback loss measurements for the membrane and oxide-clad PhC waveguides at the minimum loss wavelengths of 1557 nm and 1536 nm respectively as indicated in Fig. 3. As described in the text, the data is corrected to account for the loss in the access waveguides. (b) Experimental (solid curves) and simulated (dashed curves) propagation loss plotted as a function of the group index calculated from the dispersion curves in Fig. 2. The experimental uncertainties shown in Fig. 3 have been omitted for clarity.

#101180 - $15.00 USD Received 5 Sep 2008; revised 8 Oct 2008; accepted 8 Oct 2008; published 10 Oct 2008

4. Analysis of losses

Higher propagation losses for the air membrane devices are reported here than published previously [2] (12 dB/cm vs. 4 dB/cm). This is a consequence of the smaller writefield (100 µm x 100 µm) of the EBL system used- Raith Elphy Plus/ZEISS 1530- which introduces stitching errors that increase the propagation loss. The waveguides in [2] were fabricated using a Vistec EBPG-5 with a 600 µm x 600 µm writefield. In the present paper the absolute loss figures are less important, since we are interested in the comparison between the air membranes and the oxide-clad devices. Naïvely, one might expect the oxide-clad waveguides to perform better, given that scattering loss scales as the square of the refractive index contrast, $\alpha \approx \Delta n^2$ [10]. This is clearly not the case, however, for reasons that we now discuss.

At frequencies below the lightline, the main sources of loss in planar PhCs are surface roughness on the inside surfaces of the holes as well as random variations in the hole position and/or size. Current PhC fabrication methods can achieve disorder on the nanometre level, which is sufficiently low that the different forms of disorder can be treated as equivalent perturbations to the local refractive index on the hole boundaries. For a given level of disorder, the propagation loss depends not only on the index contrast, but also on the group velocity of the mode, and the field intensity on the etched surfaces [1, 10, 11]. Both of these contribute to the increased loss in the oxide-clad waveguides.

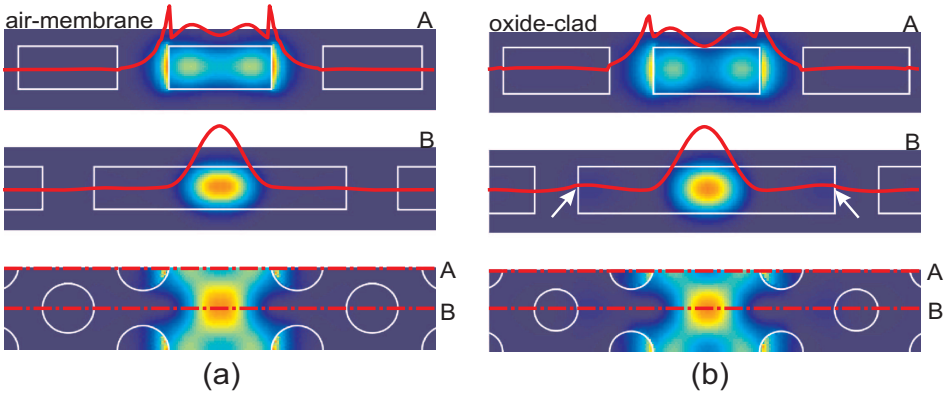

Fig. 5. Electric field intensity $|E|^2$ of the fundamental waveguide mode in (a) air-membrane and (b) oxide-clad PhC waveguides at the lowest loss wavelengths. The bottom figures in (a) and (b) show the mode profile in the centre of the Si slab, and the top and middle figures show mode cross-sections through the slab indicated by the red dashed-dotted lines. The solid red curves show the field intensity along the centerline of each figure. The white arrows indicate the increase in field intensity on the boundary of the second row of holes of the oxide-clad waveguides.

First, as can be seen in Fig. 2, the presence of the oxide moves the cladding lightline to lower frequencies, so full confinement can only be achieved for frequencies close to the cutoff of the W1 waveguide mode, where the group velocity is lower and the losses are higher. [1, 11, 12]. In fact, when compared at a group velocity corresponding to the minimum loss in the oxide-clad waveguide, the two geometries exhibit almost equal losses as shown in Fig. 4(b). Moreover, both the numerical and experimental results show that at group velocities between c/10 and c/15, the loss of the oxide-clad waveguides is slightly lower than that of the air-membranes. Second, the mode changes shape because of the reduced index contrast between the silicon and the oxide-filled holes, which increases the field overlap with the perturbation [1, 10, 11]. The difference in mode profiles is illustrated in Fig. 5, which shows the electric field intensity in the two geometries calculated at the lowest loss wavelengths indicated in Fig. 3. The fields are normalized such that the energy flux in the two waveguides is equal. While the difference is subtle, it can be seen that the oxide-clad waveguide mode extends further from the waveguide core, and there is a corresponding increase in the field intensity on the

#101180 - $15.00 USD Received 5 Sep 2008; revised 8 Oct 2008; accepted 8 Oct 2008; published 10 Oct 2008

walls of the first two rows of holes. Perhaps the most obvious difference can be seen in the middle two figures labeled "B", which show the mode in the oxide clad waveguide spreading out beyond the first row of holes as indicated by the white arrows in Fig. 3(b).

While this qualitative analysis explains the increased loss, quantitative results can only be obtained with full numerical loss simulations. Modeling nanometer scale disorder in photonic structures is a challenging task, as it typically requires high accuracy and multiple realizations of randomized structures. For such problems perturbative treatments of disorder can provide an efficient alternative to fully numerical simulations of disordered structures. Here we use such a treatment based on the GME method, which is an accurate and efficient technique that has been shown to provide good agreement with experimental results [7, 11, 13]. The disorder was modeled as a Gaussian probability distribution of hole radius with mean r_0 determined by the experimental values given earlier, and the RMS deviation Δr is used as a fitting parameter to match the measured propagation loss.

The dashed curves in Fig. 3 show the calculated loss spectra for the two waveguide geometries, where the oxide cladding index was taken to be $n_{silica} = 1.4$, a value obtained via optical reflectance measurements on the deposited FOx layer. For the membrane waveguides, a radius disorder of $\Delta r = 1.7$ nm was found to give the best fit to the experimental data, while for the oxide-clad waveguides the best fit was obtained for $\Delta r = 1.4$ nm. Although the precise value of the roughness parameter Δr might depend on the disorder model, the variation from one structure to the other should be to a large extent model-independent. While small, the difference between the two fitted roughness values is somewhat unexpected; apart from experimental uncertainty, we suspect that the FOx deposition process may cause some sidewall smoothing, thus providing a beneficial effect on the losses. Given the sub-nanometer difference in roughness, however, it was not possible to verify this by SEM inspection. The excellent agreement between the simulated and measured loss spectra in Fig. 3 is evidence of the high quality in-filling of the holes by the FOx layer. Slight differences in the shape of the loss spectra are thought to be due to additional losses introduced by writefield stitching errors which are not accounted for in the numerical analysis.

5. Conclusion

Oxide-clad PhC waveguides have many advantages over membrane structures due to their mechanical stability and ease of integration with electronic components on a single chip. We have demonstrated their successful operation and highlighted that there is an approximate threefold increase in propagation loss due to the reduced group velocity and increased overlap of the modal field with the hole surfaces. Given that the lowest reported losses in air membrane photonic crystal waveguides are well below 5 dB/cm [1-3], losses of 10-15 dB/cm may therefore be achieved in such oxide-clad waveguides. Additional improvements to the bandwidth and losses may also be achieved by tuning parameters such as the waveguide width [7, 14]. Furthermore, at equal group velocities the oxide-clad waveguides exhibit similar losses to the membrane structures, suggesting they may be particularly suited to slow-light applications. These results therefore demonstrate that the oxide-clad geometry provides a favorable alternative to membrane PhC waveguides.

Acknowledgments

The authors are grateful to M. Belotti for determining the FOx refractive index by optical measurements. T.P. White is supported by the EU-FP6 Marie Curie Fellowship project "SLIPPRY", L. O'Faolain is supported by the EU-FP6 Network of Excellence "ePIXnet" and J. Li was supported by the International Program Fund of 985 Project of Sun Yat-Sen University.

#101180 - $15.00 USD Received 5 Sep 2008; revised 8 Oct 2008; accepted 8 Oct 2008; published 10 Oct 2008